Supplementary Figures

Fig. S1. Gene Targeting at the *Hoxa3* locus. (**A**) The upper line depicts the targeting vector containing 10.1kb of genomic DNA (solid bar) encompassing the two protein-coding exons (striped boxes) of *Hoxa3*. A loxP site was inserted into the intron, destroying the native BamHI site (B) and introducing a novel EcoRV site (E). A second lox P site was inserted at an ApaI (A) site immediately 3' of the termination codon in the 3'UTR. Adjacent to this loxP site is an FRT-flanked neo^r gene. These sequences were cloned into a pUC9-based vector containing the HSV-TK gene for negative selection. The second line indicates the native *Hoxa3* locus. The third line is the $Hoxa3^{neo}$ locus generated by homologous recombination between the targeting vector and the endogenous locus. The fourth line shows the $Hoxa3^{fx}$ locus created after deletion of the neo^r sequences by action of FLP recombinase. The position of the flanking probe used to screen the ES cells is indicated, as are the sizes of the predicted DNA fragments following digestion with EcoRV. The wild-type *Hoxa3* locus resides on an EcoRV site of >20kb; targeted insertion of the 5'loxP site generates a fragment of 5.9kb. (**B**) Homologous recombination between the targeting vector and the *Hoxa3* locus was detected by Southern transfer analysis. Shown is the primary analysis of DNA isolated from two ES cell lines: the cell in lane A is homozygous for the wild-type locus; lane B shows a line heterozygous for the $Hoxa3^{neo}$ allele. (**C**) PCR genotyping gel that depicts the new $Hoxa3^{-/-}$ allele, $Hoxa3^{del}$, that was produced by crossing the $Hoxa3^{fx}$ conditional allele and a B6Cg-Tg(TeK-cre)12Flv/J female. Lane A shows a heterozygote and lane B shows a wild-type homozygote. (**D**) qRT-PCR assay of the $Hoxa3^{del}$ null allele that was produced by crossing the $Hoxa3^{fx}$ conditional allele and a B6Cg-Tg(TeK-cre)12Flv/J

female in wild-type (n=3), heterozygous (n=3), and homozygous null (n=3) embryos. The *Hoxa3*^{neo} and *Hoxa3*^{del} alleles are phenotypically indistinguishable, and were both used in this study and are referred to generically throughout the paper as *Hoxa3*$^{-}$.

Fig. S2. Characterization of the early endoderm-specific deletion mutant primordium. (**A**) HOXA3 expression of E10.5 sagittal sections from the 3rd pharyngeal region (n=2). These embryos are from pregnant *Foxa2Cre*^{ERT2} females that had intraperitoneal (IP) injections of tamoxifen in corn oil at E5.5 and E6.5. The two sections for each group are from the same embryo to show the range of variability of deletion within an embryo. DAPI is in blue. (**B**) An immunofluorescent-stained sagittal section at 42ss (~E11.25) co-stained with antibodies against FOXN1 (red), GCM2 (green), and HOXA3 (teal) (n=2). Insets show higher magnifications of the ventral tip of the primordium. *, HOXA3+ cells that are FOXN1-. Arrow indicates a FOXN1+/HOXA3+ cell. (**C**) Transverse sections of control (n=2) and endoderm deletion (n=2) embryos with antibodies against K5 and K8, or IKAROS and pan-Cytokeratin at E12.5. (**D**) Sagittal sections of control and endoderm deletion embryos at E12.0 (n=3) and at E13.5 (n=3) with antibodies against FOXN1 (red) and CC3 (green). DAPI is in blue. In all sections, anterior is up. Scale bars, 40 μm.

Fig. S3. *Ptch1* and *Fgf8* have normal expression patterns in the *Hoxa3*$^{-/-}$ mutant and the NCC deletion of *Hoxa3*, respectively. (**A,B**) E10.5 transverse sections of the 3rd pp from control and *Hoxa3*$^{-/-}$ embryos stained for *Ptch1*^{lacZ} expression (n=2). (**C,D**) E10.5 sagittal paraffin sections from control (*Hoxa3*$^{fx/-}$*;Wnt1Cre*$^{0/0}$) and NCC deletion (*Hoxa3*$^{fx/-}$

;Wnt1Cre$^{tg/0}$) embryos were subjected to ISH with a *Fgf8* riboprobe (n=2). Though the plane of section for the *Fgf8* staining shown in Figure 9 are different, each clearly shows either a difference (as in null versus endoderm deletion) or a similarity (null versus NCC deletion) between the respective control and mutant. The sections provided are representative of all the sections. Scale bars, 40 µm.

Fig. S4. The NCC-specific deletion of *Hoxa3* had little effect on the thymus. (**A**) Thymi dissected from control (*Hoxa3*$^{+/fx}$*;Wnt1Cre*$^{0/0}$) (n=7) and NCC deletion (*Hoxa3*$^{fx/-}$*;Wnt1Cre*$^{tg/0}$) (n=3) newborns. Scale bar, 100 mm. (**B**) Flow cytometry graphs indicating the distribution of thymocytes with immuno-fluorescent labeled antibodies against CD4, CD8, c-kit, and CD25. (**C**) Immunofluorescence for antibodies against K8/K5/DAPI and K14/UEA1/DAPI of control (*Hoxa3*$^{fx/-}$*;Wnt1Cre*$^{0/0}$) (n=7) and NCC deletion (*Hoxa3*$^{fx/-}$*;Wnt1Cre*$^{tg/0}$) (n=3) newborn thymi. Scale bar, 80 µm. (**D**) The number of thymocytes counted from control and NCC deletion newborn thymi. Thymocyte numbers were significantly different between mutated vs. control mice ($p = 0.033$ using the Wilcoxon rank sum test). Specifically, the mutated mice tended to have lower levels (median: 2.8; range: 0.95 to 3.7) than the control mice (median: 4.3; range: 2.9 to 9.1). To accommodate the potential influence of intra-litter correlations for these mice (i.e. mice within the same litter tend to be more similar than those not in that litter and thus are not independent), we also explored the impact of mutation (vs. control) in these mice using a GEE model that incorporates litter and the potential intra-litter correlation between mice into that evaluation. While our numbers are very limited for this more complex model,

we did find that this also showed a significant influence *Hoxa3* deletion in NCCs ($p<0.0001$).

Fig. S5. The tissue-specific deletions of *Hoxa3* have thymus-pharynx detachment defects. (**A,D**) Immunofluorescence for antibodies against P63 and DAPI of E12.5 sagittal sections of a control (*Hoxa3*$^{+/fx}$*;Foxa2*$^{CreERT2/+}$) (n=2) and an endoderm deletion (*Hoxa3*$^{fx/-}$*;Foxa2*$^{CreERT2/+}$) (n=2) embryo. (**B,E**) H&E-stained E14.5 transverse sections of control (n=2) and endoderm deletion embryos (n=3). (**C,F**) TUNEL staining (green) on E11.5 sagittal sections of control (*Hoxa3*$^{fx/+}$*; Wnt1Cre*$^{0/0}$) (n=3) and NCC deletion (*Hoxa3*$^{fx/-}$*;Wnt1Cre*$^{tg/0}$) (n=3) embryos. Regions between the dotted lines indicate the thymus-pharynx connection zone. The primordium and pharynx of the NCC deletion mutant has fewer apoptotic cells within the endoderm of the thymus-pharynx region than in the control. (**G,H**) 3D reconstruction of a NCC deletion newborn pharynx (yellow), thymus (blue) and parathyroid (red). G and H show different angles of the same 3D reconstruction so that the reader can see the connection points between the parathyroid and thymus (G, white arrows) and between the thymus and the pharynx (H, arrowhead). thy, thymus. pt, parathyroid. phx, pharynx. Scale bars, 40 μm.

Fig. S6. *Gcm2* and *Pth* have normal expression patterns in the parathyroid conditional deletion of *Hoxa3*. E13.5 transverse sections subjected to ISH with a *Pth* and a *Gcm2* riboprobe in *Hoxa3*$^{+/fx}$*;Pth*$^{Cre/+}$ and *Hoxa3*$^{fx/-}$*;Pth*$^{Cre/+}$ embryos (n=2 for each probe and each genotype). Scale bar, 80 μm.

Fig. S7. The smaller thymus in the thymus-specific deletion of *Hoxa3* differentiated normally. (**A**) The number of thymocytes for two (P-value=0.09) and four (P-value=0.06) week old thymi is not significantly different after Foxn1Cre-mediated deletion (*Hoxa3*$^{fx/-}$*;Foxn1*$^{Cre/+}$) (n=3) compared to the control (*Hoxa3*$^{+/fx}$*;Foxn1*$^{+/+}$) (n=6). (**B**) Immunofluorescence for antibodies against K8/K5/DAPI and K14/UEA1/DAPI of *Hoxa3*$^{fx/-}$*;Hoxd3*$^{+/+}$*;Foxn1*$^{+/+}$ (n=3), *Hoxa3*$^{fx/-}$*;Hoxd3*$^{+/+}$*;Foxn1*$^{Cre/+}$ (n=1), and *Hoxa3*$^{fx/-}$*;Hoxd3*$^{+/-}$*;Foxn1*$^{Cre/+}$ (n=1). Scale bar, 80 μm. (**C**) Flow cytometry graphs indicating the distribution of thymocytes with immuno-fluorescent labeled antibodies against CD4, CD8, c-kit, and CD25. (**D**) PCR of *Hoxa3*, *Hoxd3*, or *β-actin* (control) in CD45+(thymocytes), CDR1- (mTECs), CDR+ (cTECs), or water (control). Neither *Hoxa3* nor *Hoxd3* are expressed in thymocytes, but both are expressed in cTECs while only *Hoxa3* is expressed in mTECs.

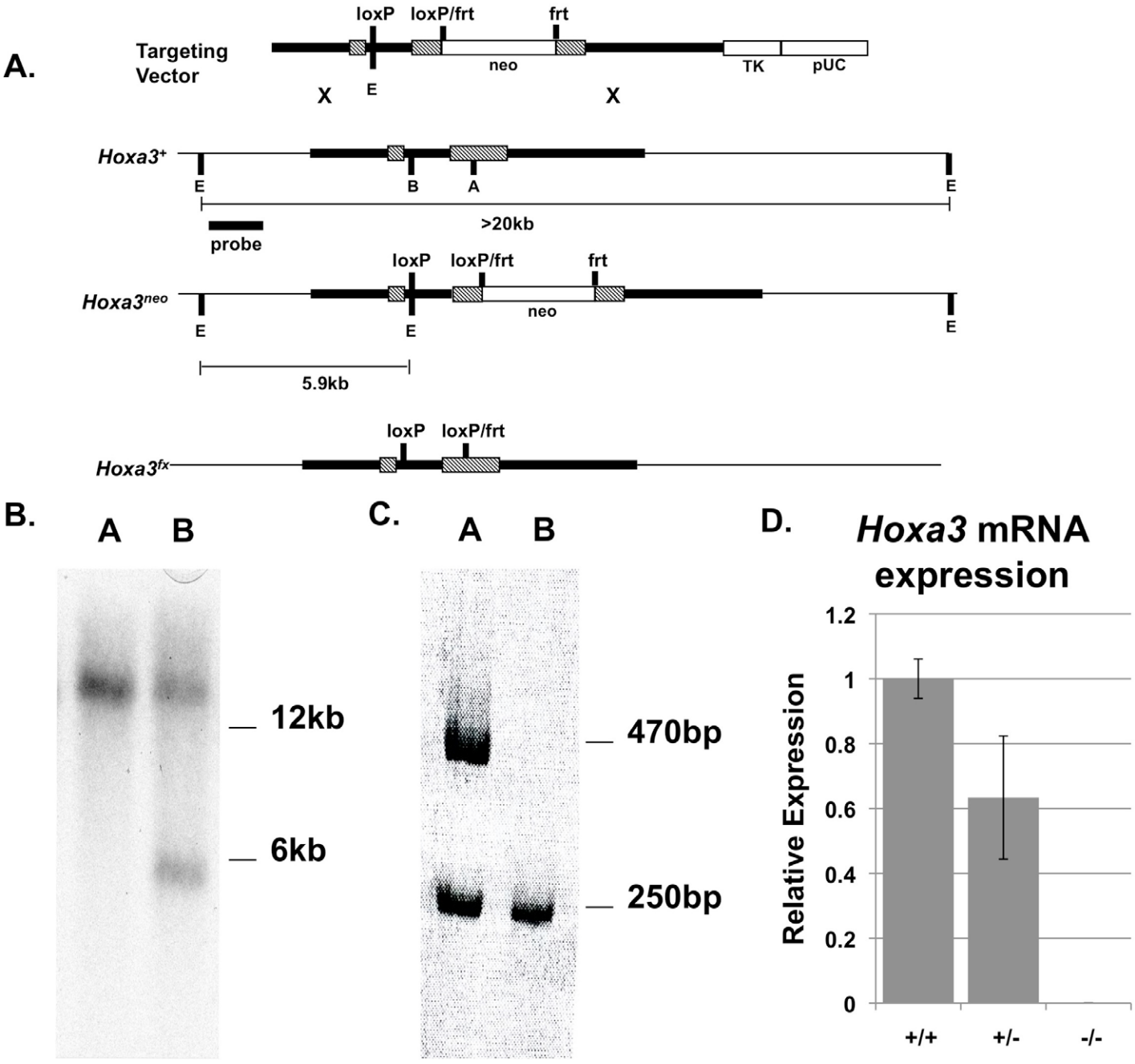
A.
Targeting Vector
loxP
loxP/frt
frt
neo
TK
pUC
X
E
X
Hoxa3+
E
B
A
E
>20kb
probe
loxP
loxP/frt
frt
Hoxa3neo
neo
E
E
E
5.9kb
loxP
loxP/frt
Hoxa3fx
B.
A
B
12kb
6kb
C.
A
B
470bp
250bp
D.
Hoxa3 mRNA expression
Relative Expression
1.2
1
0.8
0.6
0.4
0.2
0
+/+
+/-
-/-

Figure S1.

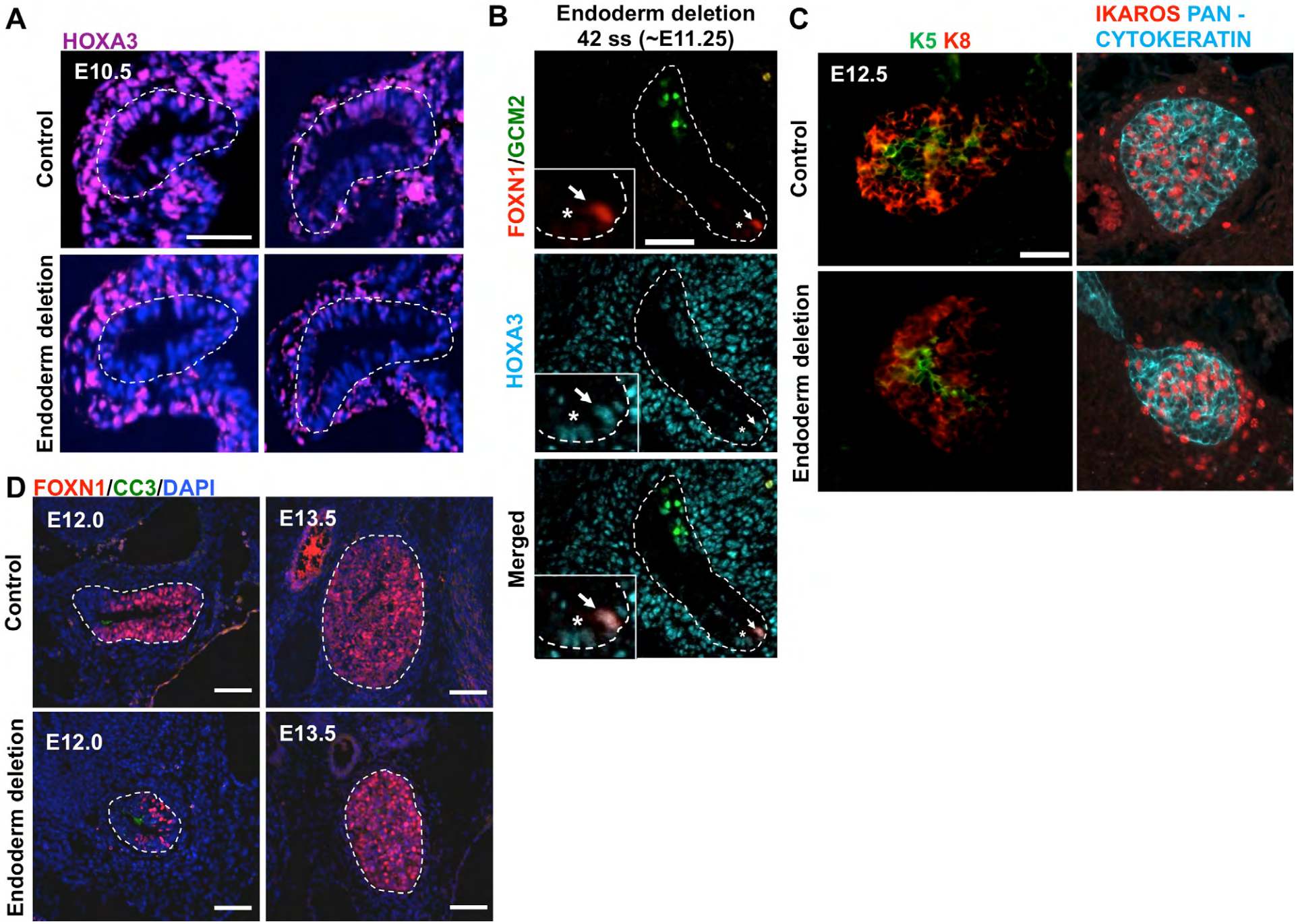
A
HOXA3
E10.5
Control
Endoderm deletion
B
Endoderm deletion
42 ss (~E11.25)
FOXN1/GCM2
HOXA3
Merged
C
K5 K8
IKAROS PAN -
CYTOKERATIN
E12.5
Control
Endoderm deletion
D
FOXN1/CC3/DAPI
E12.0
E13.5
Control
Endoderm deletion

Figure S2.

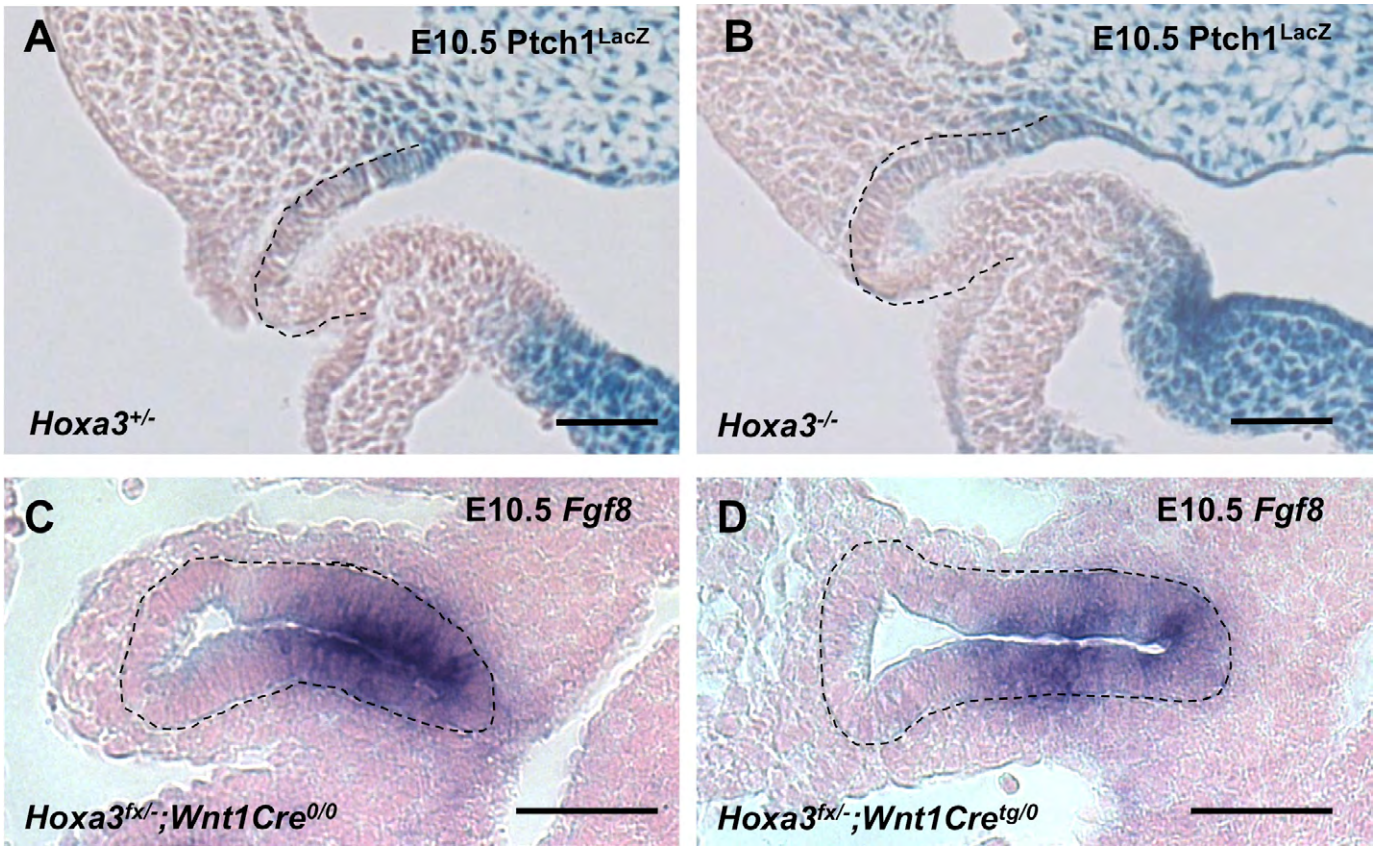
A
E10.5 Ptch1LacZ
Hoxa3+/-
B
E10.5 Ptch1LacZ
Hoxa3-/-
C
E10.5 Fgf8
Hoxa3fx/-;Wnt1Cre0/0
D
E10.5 Fgf8
Hoxa3fx/-;Wnt1Cretg/0

Figure S3.

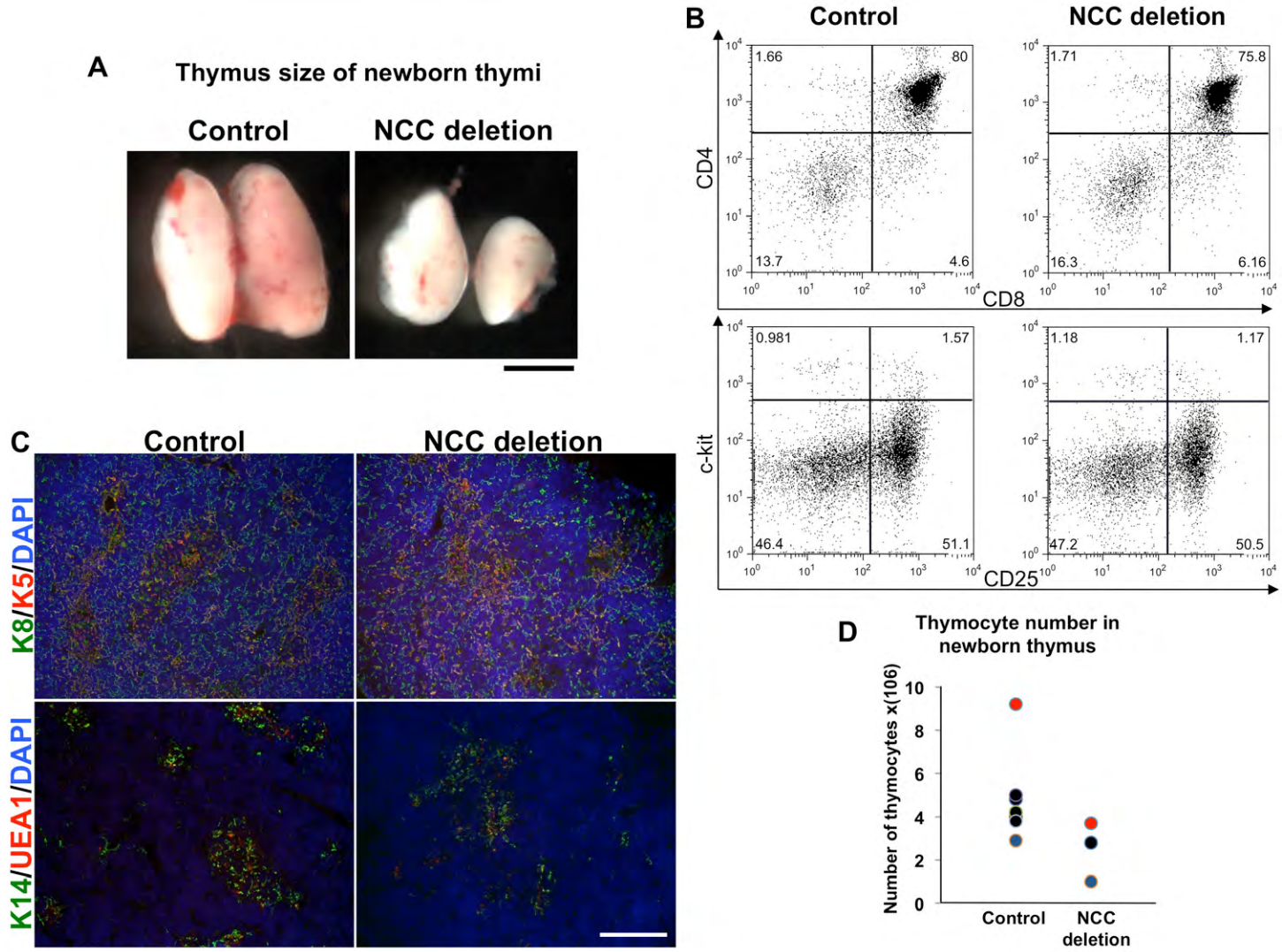
A
Thymus size of newborn thymi
Control
NCC deletion
B
Control
NCC deletion
CD4
CD8
c-kit
CD25
1.66
80
13.7
4.6
1.71
75.8
16.3
6.16
0.981
1.57
46.4
51.1
1.18
1.17
47.2
50.5
C
Control
NCC deletion
K8/K5/DAPI
K14/UEA1/DAPI
D
Thymocyte number in newborn thymus
Number of thymocytes x(10^6)
Control
NCC deletion

Figure S4.

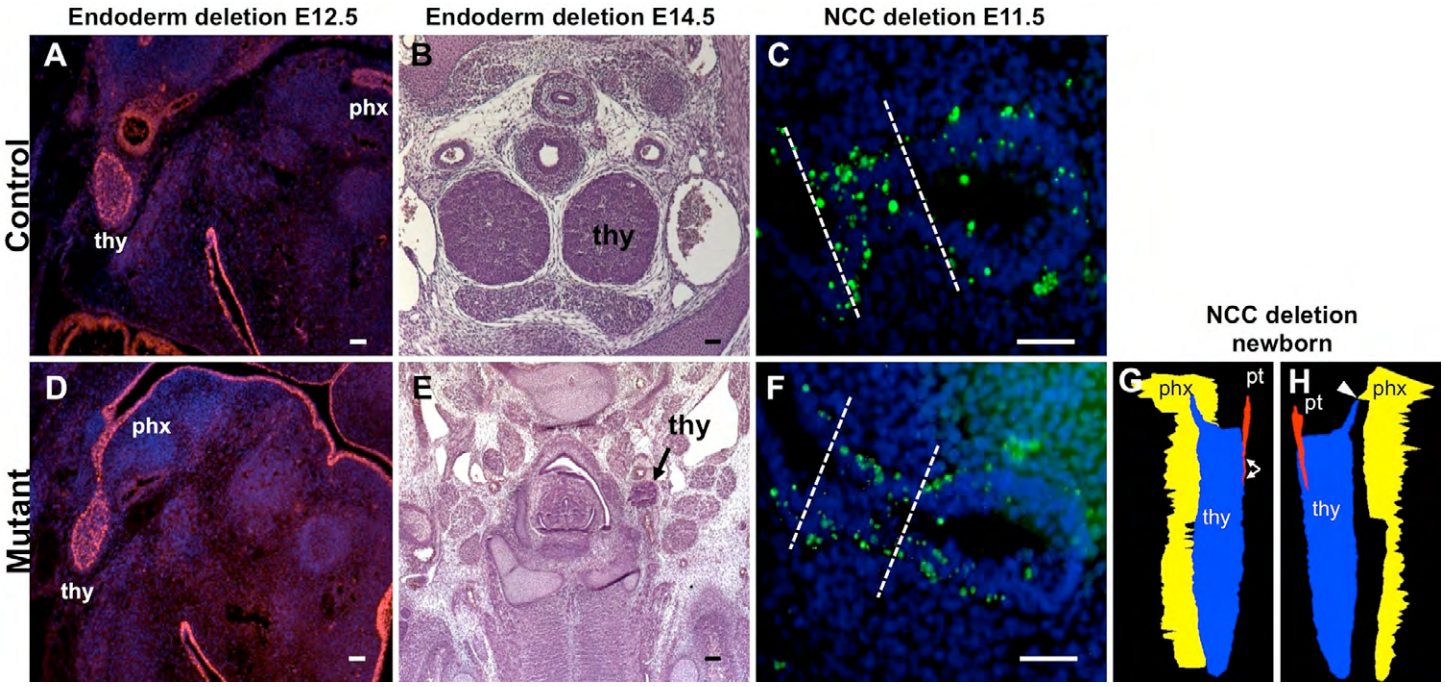
Endoderm deletion E12.5
Endoderm deletion E14.5
NCC deletion E11.5
NCC deletion newborn
Control
Mutant
A
B
C
D
E
F
G
H
phx
thy
pt

Figure S5.

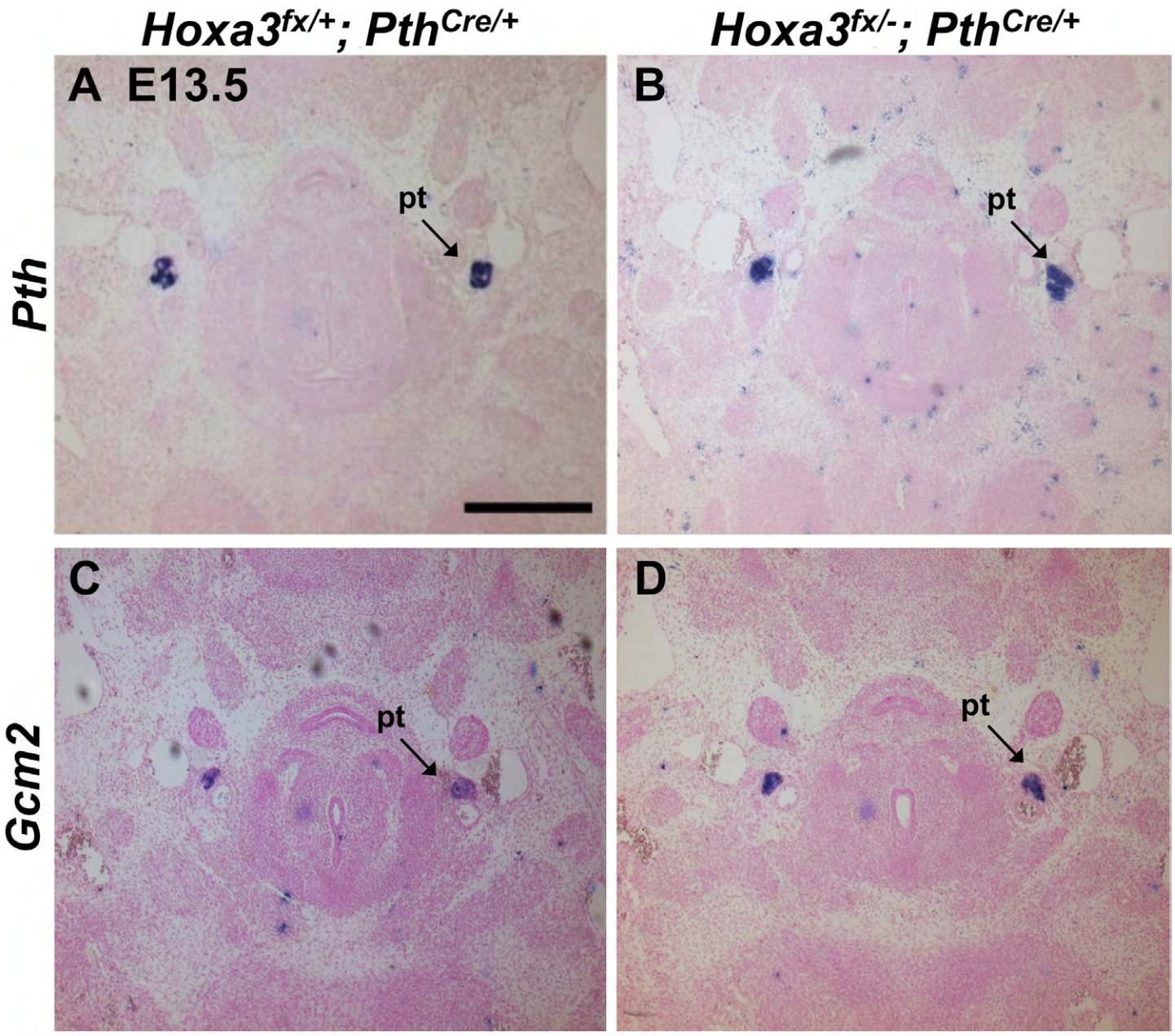

Figure S6.

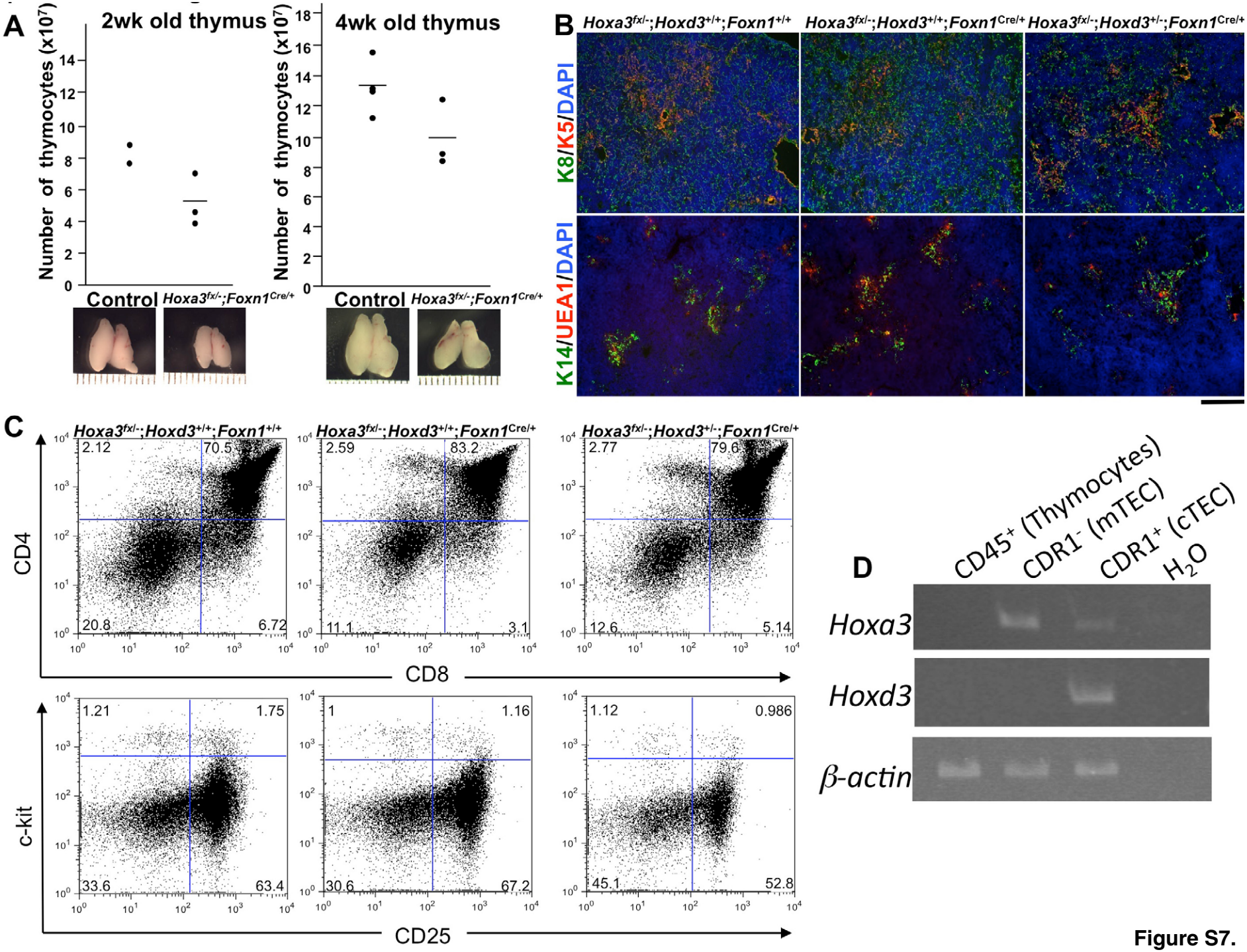
A
2wk old thymus
4wk old thymus
Number of thymocytes (x10^7)
Control
Hoxa3fx/-;Foxn1Cre/+
B
Hoxa3fx/-;Hoxd3+/+;Foxn1+/+
Hoxa3fx/-;Hoxd3+/+;Foxn1Cre/+
Hoxa3fx/-;Hoxd3+/-;Foxn1Cre/+
K8/K5/DAPI
K14/UEA1/DAPI
C
CD4
CD8
c-kit
CD25
2.12
70.5
20.8
6.72
2.59
83.2
11.1
3.1
2.77
79.6
12.6
5.14
1.21
1.75
33.6
63.4
1
1.16
30.6
67.2
1.12
0.986
45.1
52.8
D
CD45+ (Thymocytes)
CDR1- (mTEC)
CDR1+ (cTEC)
H2O
Hoxa3
Hoxd3
β-actin

Figure S7.